The 2010 IEEE/RSJ International Conference on
Intelligent Robots and Systems
October 18-22, 2010, Taipei, Taiwan

Trajectory Planning of a One-Legged Robot Performing Stable Hop

Ting-Ying Wu, T.-J. Yeh and Bing-Hung Hsu

Abstract— **In this paper, stable hopping of a one-legged, articulated robot with a flat foot is investigated. The robot has a special feature that before taking off, it goes through an underactuated phase in which the foot rotates about the unactuated toe on the ground. By having the underactuated phase, the robot can perform stable human-like hops with longer hopping distances. To devise a systematic trajectory design methodology for the robot, its dynamics including the ground-foot impact and the hopping constraints are carefully studied. An optimization procedure is then proposed to plan the feasible actuated trajectories which not only meet specific performance requirements but also attain certain optimality with respect to actuation energy. The hopping strategy and the optimal trajectories are verified by simulations and hardware implementation. Experiments indicate that the robot not only can stably perform hops with different hopping distances on the level ground but also can successfully hop up/down staircases.**

I. Introduction

Through hopping and jumping, legged robots can demonstrate their dexterity and mobility. During 1980's, Raibert et al. first developed one-legged [1] and two-legged [2] hopping robots. These robots had telescopic legs, point feet, and used pneumatic or hydraulic cylinders for actuation. They were also equipped with control algorithms for controlling forward velocity, hopping height and body attitude. Recently, to achieve stable jumping or hopping, there has been a growing interest in incorporating articulated legs and flat feet to the robots. With the flat feet, the robots can maintain dynamic stability in the support/stance phase by controlling the zero-moment-point (ZMP) to be within the non-negligible foot area. For instance, the authors in [3] developed a 7 DOF, one-legged robot with an actuated toe joint. By solving the discretized ZMP equations in real time, the robot can hop with a maximal height of $4\,\mathrm{cm}$ and turn around by rotating the hip in the yaw direction during the flight phase.

In normal human jumping, right before the takeoff, there is an underactuated phase that the foot rotates around the passive toe joint. To explore underactuation feature of human jumping, Kajita et al. added passive toe joints with torsional springs to the HRP-2LT [4] robot. The ZMP trajectory is pre-specified that the ZMP starts from the foot center, then gradually moves to the toe link to initiate underactuated rotation in the passive toe joint, and finally moves and stays at the toe tip to initiate another underactuated rotation around the toe tip before the robot completely takes off. Regardless that it was validated in simulations that the robot can achieve more effective jumping and running with added toe joints and springs, only a preliminary experiment on vertical hopping was shown.

In this research, an articulated, one-legged robot with two actuated joints and a flat foot is developed to perform stable hop. Although for simplification the developed robot does not have the toe link, similar to the work in [4], the hopping of the robot also undergoes an underactuated phase as in the normal human jumping. For fully exploiting the dynamics for the specific hopping characteristics of the robot developed, an optimization procedure is proposed to systematically determine the actuated joint trajectories throughout the hopping process. By carefully considering all the possible constraints including impact minimization and motor specifications, the procedure can lead to feasible actuated trajectories which are directly ready for experimental implementation. The rest of the paper is devoted to analysis and hardware implementation of a one-legged robot peforming stable hops.

II. Dynamics for the One-Legged Hopping Robot

The photo of the one-legged robot and its schematic model are shown in Fig. 1. The robot contains three links which respectively correspond to the foot, the leg and the torso. There are an ankle joint connecting the foot and the leg, and a hip joint connecting the leg and the torso. Each of the two joints is actuated by an electrical motor with gear transmission.

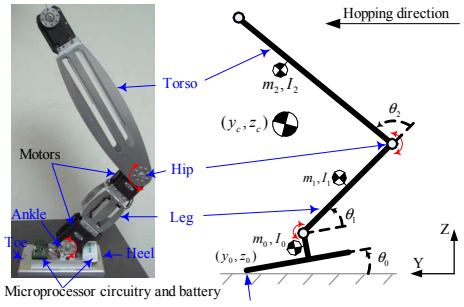

Fig. 1. The photo and the schematic model of the one-legged robot with definitions of critical varibles for dynamic analysis.

In Fig. 2, the stick diagrams of the one-legged robot performing stable hop in a cycle are shown in the sagittal view. One hopping cycle consists of six consecutive postures 1~6: Initially, at posture 1, the robot stands statically and prepares to crouch down for hopping. Its foot is flatly in contact with ground and the center of pressure (CoP) of the foot-ground contact force is located around the center of the

Ting-Ying Wu, T.-J. Yeh and Bing-Hung Hsu are with the Department of Power Mechanical Engineering, National Tsing Hua University, Hsinchu, Taiwan 30013, R.O.C. d927706@oz.nthu.edu.tw ;tyeh@pme.nthu.edu.tw ; imagine1985430@hotmail.com

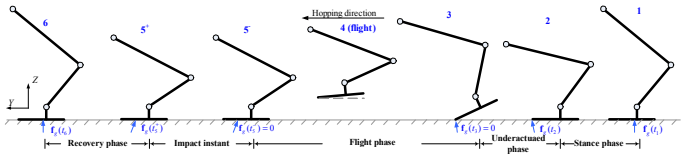

Fig. 2. Stick diagrams of the one-legged robot in a hopping cycle.

foot. At posture 2, the CoP just moves to the toe, and the foot is about to rotate about the toe to raise the center of mass (CoM) further forward and upward. At posture 3, the foot has rotated, and the foot-ground contact force just vanishes that the foot is about to leave off the ground completely. At posture 4, the foot has been lifted off the ground and the robot is flying in the air. At posture 5, the foot just flatly lands on the ground, and impact occurs between the foot and the ground. The superscripts $-$ and $+$ for this posture respectively represent the instants just before and right after foot-ground impact. Finally, at posture 6 the robot recovers its initial posture and stands statically again.

Let t_i denote the time instant while the i^{th} posture occurs. From t_1 to t_2 and from t_5 to t_6, which are respectively referred to as the stance phase and the recovery phase, the robot's foot flatly stays on the ground without any sliding and rotation. The robot has 2 DOF and is fully actuated in these phases. From t_2 to t_3, the foot rotates freely about the toe which itself can be viewed as a free joint, so the robot has 3 DOF. With only two actuated joints, such a duration is referred to as the underactuated phase. From t_3 to t_5, the robot is completely lifted off the ground and is referred to be in the flight phase. In this phase, other than three rotational DOF, translations in the y and the z axes also occur, so totally the robot has 5 DOF.

For generality, all the five possible DOF motion is considered in the model shown in Fig. 1. Among the symbols depicted, m_i $(i = 0, 1, 2)$ represents the mass of link i, I_i is the associated moment of inertia about the center of mass of the link, θ_2, θ_1 and θ_0 respectively denote the hip angle, the ankle angle, and the angle around the toe, y_0 and z_0 are the translational displacements of the toe respectively along the y and z axes, and finally (y_c, z_c) is the coordinates for the CoM of the robot.

Using $\mathbf{q} = [y_0 \ z_0 \ \theta_0 \ \theta_1 \ \theta_2]^T$ as generalized coordinates, the 5 DOF motion of the proposed robot can be described by the following equation:

$$\mathbf{M}(\mathbf{q})\cdot\ddot{\mathbf{q}} + \mathbf{C}(\mathbf{q}, \dot{\mathbf{q}})\cdot\dot{\mathbf{q}} + \mathbf{g}(\mathbf{q}) = \boldsymbol{\tau} + \mathbf{J}(\mathbf{q})^T\cdot\mathbf{f}_g \ . \quad (1)$$

In this equation, $\mathbf{M}$ is the inertia matrix, $\mathbf{C}$ is a matrix related to the Coriolis and centrifugal effects, $\mathbf{g}$ is the gravitational torque vector, and $\boldsymbol{\tau} = [0 \ 0 \ 0 \ \tau_1 \ \tau_2]^T$ is a controlled torque vector, in which τ_1 and τ_2 corresponding to the torques respectively generated by the ankle and the hip motors. Finally, $\mathbf{f}_g$ is the vector representing the interaction force/moment between the foot and the ground with $\mathbf{J}(\mathbf{q})$ being the associated Jacobian matrix. Note that except for $\mathbf{f}_g = \mathbf{0}$ in flight phase, the interaction point of $\mathbf{f}_g$ must be located inside the support area of the foot (during the stance phase and the recovery phase) or at the toe (during the underactuated phase).

By the special structure in $\boldsymbol{\tau}$, (1) can be partitioned as follows:

$$\mathbf{M}_u(\mathbf{q})\cdot\ddot{\mathbf{q}} + \mathbf{C}_u(\mathbf{q}, \dot{\mathbf{q}})\cdot\dot{\mathbf{q}} + \mathbf{g}_u(\mathbf{q}) = \mathbf{0} + \mathbf{J}_u(\mathbf{q})^T\cdot\mathbf{f}_g \quad (2)$$

$$\mathbf{M}_a(\mathbf{q})\cdot\ddot{\mathbf{q}} + \mathbf{C}_a(\mathbf{q}, \dot{\mathbf{q}})\cdot\dot{\mathbf{q}} + \mathbf{g}_a(\mathbf{q}) = \boldsymbol{\tau}_a \ . \quad (3)$$

In the above two equations, the subscripts u and a respectively denote the unactuated and actuated parts of the vector/matrix, $\boldsymbol{\tau}_a = [\tau_1 \ \tau_2]^T$, and $\mathbf{q}$ is implicitly composed of $\mathbf{q}_u = [y_0 \ z_0 \ \theta_0]^T$ and $\mathbf{q}_a = [\theta_1 \ \theta_2]^T$. Note that since $\mathbf{f}_g$ must acts on the ground surface, the associated Jacobian should vanish along the direction of $\mathbf{q}_a$, or $\mathbf{J}(\mathbf{q}) = [\mathbf{J}_u(\mathbf{q}) \ \mathbf{0}]$.

The robot has 2 DOF actuation, so the trajectory of $\mathbf{q}_a$, if feasible in terms of the constraints discussed in the next section, can be directly controlled. On the other hand, $\mathbf{q}_u$, which constitutes the unactuated part of the generalized coordinates, is the result of the dynamic interaction between the controlled trajectories and the mechanism dynamics. In the following, the solution of $\mathbf{q}_u(t)$ to a given feasible trajectory of $\mathbf{q}_a(t)$ in different phases is studied.

- **Stance phase:** During this phase, the foot flatly stays on the ground without sliding and rotation, so $\mathbf{q}_u$ is motionless or can be simply written as

$$\mathbf{q}_u(t) = \begin{bmatrix} 0 & 0 & 0 \end{bmatrix} \ , \ t \in [t_1, t_2] \ . \quad (4)$$

- **Underactuated phase:** During the underactuated phase, it is assumed that the foot rotates freely about the toe and the toe does not slide. This leads to the condition that for $t \in [t_2, t_3]$, the third component of $\mathbf{J}_u(\mathbf{q})^T\cdot\mathbf{f}_g$ in the equation of (2) vanishes, and $y_0(t) = z_0(t) = 0$. Therefore, given a feasible $\mathbf{q}_a(t)$, the third equation in (2) can be numerically integrated to solve for $\theta_0(t)$, consequently $\mathbf{q}_u(t)$. Here an operator $\boldsymbol{\Gamma}_{\mathbf{q}_{23}}$ is used to denote the functional dependency between $\mathbf{q}_u$ and $\mathbf{q}_a$ during the underactuated phase, or

$$\mathbf{q}_u(t) = \boldsymbol{\Gamma}_{\mathbf{q}_{23}}(\mathbf{q}_a(t)) \ , \ t \in [t_2, t_3] \ . \quad (5)$$

- **Flight phase:** During the flight phase, no external force except gravity is exerted on the robot, so the dynamics follow the conservation of linear and angular momentums as

$$\begin{cases} \dot{y}_c(t) = \dot{y}_c(t_3) \\ \dot{z}_c(t) = \dot{z}_c(t_3) - g(t - t_3) \\ H_{CoM}(t) = H_{CoM}(t_3) \end{cases} , \ t \in [t_3, t_5] \quad (6)$$

where g is the gravitational acceleration, and $H_{CoM}(t)$ is the angular momentum about the CoM of the robot. In these equations, by kinematic analyses $\dot{y}_c$, $\dot{z}_c$, as well as H_{CoM} can be represented as functions of $\mathbf{q}$ and $\dot{\mathbf{q}}$. Thus (6) can be written in the following form:

$$\mathbf{H}(\mathbf{q}(t))\,\dot{\mathbf{q}}(t) = \mathbf{H}(\mathbf{q}(t_3))\,\dot{\mathbf{q}}(t_3) + [0 \ g(t_3 - t) \ 0]^T \quad (7)$$

where $\mathbf{H}$ is a 3×5 matrix that relates the generalized velocity $\dot{\mathbf{q}}$ to $\dot{y}_c$, $\dot{z}_c$, and H_{CoM}. Since $\mathbf{q}_a(t)$ is given

and $\mathbf{q}(t_3)$ and $\dot{\mathbf{q}}(t_3)$ can be obtained as the final states of the underactuated phase, (7) can be integrated to numerically solve for $\mathbf{q}_u(t)$. Here an operator $\mathbf{\Gamma}_{\mathbf{q}_{35}}$ is used to denote the functional dependency between $\mathbf{q}_u$ and $\mathbf{q}_a$, or

$$\mathbf{q}_u(t) = \mathbf{\Gamma}_{\mathbf{q}_{35}}(\mathbf{q}_a(t)) \ . \tag{8}$$

- **Recovery phase**: In this phase the foot flatly stays on the ground without sliding and rotation as the stance phase but the foot could be placed at a different location. In this case $\mathbf{q}_u$ is written as

$$\mathbf{q}_u(t) = \begin{bmatrix} l & h & 0 \end{bmatrix} \ , \ t \in [t_5, t_6] \ . \tag{9}$$

where l denotes the hopping distance, h is the final hopping height with $h > 0$ for hopping up and $h < 0$ for hopping down.

According to the above analysis, $\mathbf{q}_u(t)$ is either constant or functionally dependent on $\mathbf{q}_a(t)$. Consequently, $\mathbf{q}_a(t)$ alone dictates the dynamics of the one-legged robot. Using (2), one can directly compute the contact force/torque $\mathbf{f}_g$ in terms of $\mathbf{q}(t)$, thus $\mathbf{q}_a(t)$. An operator $\mathbf{\Gamma}_{\mathbf{f}_g}$ is used to denote the functional dependency of $\mathbf{f}_g$ on $\mathbf{q}_a(t)$, or

$$\mathbf{f}_g(t) = \mathbf{\Gamma}_{\mathbf{f}_g}(\mathbf{q}_a(t)) \ . \tag{10}$$

Similarly, an operator $\mathbf{\Gamma}_{\boldsymbol{\tau}_a}$ can be applied to show the functional dependency of the actuation torque $\boldsymbol{\tau}_a$ on $\mathbf{q}_a(t)$, or

$$\boldsymbol{\tau}_a(t) = \mathbf{\Gamma}_{\boldsymbol{\tau}_a}(\mathbf{q}_a(t)) \ . \tag{11}$$

III. Constraints for Achieving a Stable Hop

One main purpose of the paper is to devise a feasible solution for $\mathbf{q}_a(t)$ so that the robot can perform stable hop with some optimality with respect to the use of actuation energy. To do so, constraints on the trajectories are investigated. The constraints will be incorporated into the numerical procedure subsequently to determine the feasible solution for $\mathbf{q}_a(t)$. Basically, there are seven types of constraints. They are:

1) Constraints for initial and final postures: For a hopping cycle, the initial and final postures of the robot are specified by

$$\mathbf{q}(t_i) = \mathbf{q}_d^i \text{ and } \dot{\mathbf{q}}(t_i) = \mathbf{0} \ , \text{ for } i = 1,\ 6 \ , \tag{12}$$

where $\mathbf{q}_d^i$ is a given joint angle/position vector at time t_i.

2) Constraints for continuity and discontinuity: According to Fig. 2, transitions between phases occur at posture 2, 3, and 5. At these postures, the degrees of freedom of the robot change. Regardless of the change in DOF, except for posture 5, both the positions/joint angles and the corresponding velocities in the generalized coordinates should be continuous at the associated time instants. In other words,

$$\begin{cases} \mathbf{q}(t_i^-) = \mathbf{q}(t_i) = \mathbf{q}(t_i^+) \\ \dot{\mathbf{q}}(t_i^-) = \dot{\mathbf{q}}(t_i) = \dot{\mathbf{q}}(t_i^+) \end{cases} \ , \text{ for } i = 2,\ 3 \tag{13}$$

At posture 5, foot-ground impact occurs, so the continuity only holds in the positions and joint angles, or

$$\mathbf{q}(t_5^-) = \mathbf{q}(t_5) = \mathbf{q}(t_5^+) \ . \tag{14}$$

Particularly, to avoid successive impacts, it is assumed that at t_5^- the foot angle θ_0 has already been slewed to zero degree that (9) also holds for $t = t_5^-$. As for the velocities, they are discontinuous at the moment of impact. Assuming the impact is purely plastic, the linear velocities and the angular velocity of the foot should vanish. Moreover, if both sides of (3) are integrated from t_5^- to t_5^+, by the continuity in joint angles and the actuator torques ($\boldsymbol{\tau}_a$), and the instantaneous nature of the impact, we have

$$\dot{\mathbf{q}}_u(t_5^+) = \mathbf{0} \text{ and } \mathbf{M}_a(\mathbf{q}(t_5))\cdot\left(\dot{\mathbf{q}}(t_5^+) - \dot{\mathbf{q}}(t_5^-)\right) = \mathbf{0}, \tag{15}$$

which constitute the discontinuity constraint for the velocities at posture 5. One can directly compute the after-impact velocity, $\dot{\mathbf{q}}(t_5^+)$, from the before-impact velocity, $\dot{\mathbf{q}}(t_5^-)$, using these two equations.

3) Constraints for clearance: During the underactuated phase, the heel clears from the ground and the foot rotates about the toe. This is equivalent to

$$\theta_0(t) > 0 \ , \text{ for } t \in (t_2, t_3] \ . \tag{16}$$

On the other hand, during the flight phase, the foot should clear from the ground to avoid the foot-ground interference. Such a constraint is given by

$$\begin{matrix} z_0(t) > 0 \\ z_0(t) + l_{foot}\sin\theta_0(t) > 0 \end{matrix} \ , \text{ for } t \in (t_3, t_5) \ , \tag{17}$$

where the second inequality limits the height of the heel, and l_{foot} denotes the length of the foot.

4) Constraint for minimizing impact: Ideally, to eliminate the foot-ground impact at touchdown for reducing energy loss, one can simply slew the foot velocities ($\dot{y}_0$, $\dot{z}_0$, and $\dot{\theta}_0$) to zero right before the impact, or $\dot{\mathbf{q}}_u(t_5^-) = \mathbf{0}$. However, because the motions in $\dot{y}_0$, $\dot{z}_0$ are quite substantial during the shortly flight phase, it requires quite significant actuator authority to achieve $\dot{y}_0(t_5^-) = \dot{z}_0(t_5^-) = 0$. Here, as a compromise between the capacity of the motor used and the energy loss due to impact, we simply set the constraint

$$\dot{\theta}_0(t_5^-) = 0 \ . \tag{18}$$

5) Constraints for the contact force ($\mathbf{f}_g$): While the foot is in contact with the ground, two constraints for contact force need to be satisfied to hop in a stable manner. One is that sliding should not occur between the foot and the ground. Such a constraint is relevant to $\mathbf{f}_g$, which has three components: a force in y direction ($(\mathbf{f}_g)_z$), a force in z direction ($(\mathbf{f}_g)_y$), and a moment in x direction ($(\mathbf{f}_g)_x$). To prevent the foot from sliding, we should have

$$|(\mathbf{f}_g)_y| \le \mu_s(\mathbf{f}_g)_z \ , \ t \in [t_1, t_3] \text{ and } t \in [t_5, t_6] \tag{19}$$

where μ_s is the coefficient of static friction. Equation (19) also implicitly restricts $(\mathbf{f}_g)_z$ to be non-negative, which comes from the uni-directionality of the ground reaction.

The other constraint about $\mathbf{f}_g$ is imposed for the foot to flatly contact with the ground ($\theta_0(t) = 0$) during the stance phase and the recovery phase, but rotate about the toe during the underactuated phase. This constraint is equivalent to limiting the CoP associated with $\mathbf{f}_g$ to be strictly inside the foot during the stance phase and the recovery phase, and to limiting the CoP to be exactly located at the toe during the underactuated phase. These constraints are analytically given as

$$0 \leq \frac{(\mathbf{f}_g)_x}{(\mathbf{f}_g)_z} \leq l_{foot} \ , \ t \in [t_1, t_2) \tag{20}$$

$$l \leq \frac{(\mathbf{f}_g)_x}{(\mathbf{f}_g)_z} \leq l + l_{foot} \ , \ t \in (t_5, t_6] \tag{21}$$

$$(\mathbf{f}_g)_x = 0 \ , \ t \in [t_2, t_3] \tag{22}$$

6) Constraints for the CoM motion: When the robot is in flight, the only external force acting on it is gravity. The CoM should follow the projectile motion that the resultant trajectory is parabolic and is dependent on the initial speed and the projection angle. In order for the robot to achieve a maximal hopping distance with least energy, we require the take-off velocity of the CoM to have identical horizontal and vertical components, or

$$\dot{y}_c(t_3) = \dot{z}_c(t_3) > 0 \ , \tag{23}$$

7) Constraints for motors: The two DC motors used should obey some constraints. First, the gear reductions associated with the motors do not allow the joints to rotate continuously but limit the joint angles as

$$\theta_{\min} \leq \theta_i \leq \theta_{\max} \ , \text{ for } i = 1, 2 \tag{24}$$

where $\theta_{\min}$ and $\theta_{\max}$ respectively represents the lower bound and upper bound of the joint angle. Secondly, considering that if the electrical time constant of the motor is ignored, part of the input voltage to the motor coil is to counteract the back emf proportional to the motor speed, and the rest of the voltage is to generate motor torque via electro-mechanical interaction, the following constraint is imposed:

$$\frac{R}{k_m \cdot n} |\tau_i| + (k_e \cdot n) \left|\dot{\theta}_i\right| \leq v \ , \text{ for } i = 1, 2 \tag{25}$$

where k_m is the motor constant, k_e is the back emf constant, n is the gear reduction ratio, R is the coil resistance, and v is the maximum input voltage.

IV. An Optimization Procedure for Determining Joint Trajectories

To minimize the actuation energy in a hopping cycle, the performance index $J = \int_{t_1}^{t_6} \|\boldsymbol{\tau}_a(t)\|^2 \, dt$ is defined. In a DC motor, torque is proportional to current, so the electrical power is proportional to the square of the current.

By (11), the performance index can be expressed in terms of $\mathbf{q}_a(t)$. In this section, an optimization procedure is proposed to determine feasible $\mathbf{q}_a(t)$ to minimize such a performance index under the seven constraints listed previously. Because the robot experiences change in DOF at postures 2, 3 and 5, $\mathbf{q}_a(t)$ in the optimization is assumed to be a concatenation of four smooth Bèzier polynomials $\mathbf{q}_{a\_12}(t)$, $\mathbf{q}_{a\_23}(t)$, $\mathbf{q}_{a\_35}(t)$ and $\mathbf{q}_{a\_56}(t)$ respectively defined in $[t_1, t_2]$, $[t_2, t_3]$, $[t_3, t_5]$ and $[t_5, t_6]$. A typical Bèzier polynomial $\theta(t)$ is in the form of $\theta(t) = \sum_{i=0}^{m} \frac{m!}{i!(m-i)!} t^i (1-t)^{m-i} \cdot x_i$, where m is the order of the polynomial, and $\frac{m!}{i!(m-i)!} t^i (1-t)^{m-i}$ is referred to as a basis function with x_i being the associated control point. The polynomials for actuated trajectories can be generally parameterized as

$$\mathbf{q}_{a\_ij}(t) = \mathbf{A}_{ij} \mathbf{h}(t), \text{ for } t \in \left[t_i, t_j\right]$$

where (i, j)=$(1, 2)$, $(2, 3)$, $(3, 5)$ and $(5, 6)$, $\mathbf{h}(t) = [(1-t)^m \quad mt(1-t)^{m-1} \quad \cdots \quad t^m]^T$, and $\mathbf{A}_{(\cdot)}$'s are matrices constituted by control points of the associated polynomial. The optimization problem can be cast as

$$\min_{\substack{A_{12}, A_{23}, \\ A_{35}, A_{56}}} \left(\int_{t_1}^{t_2} \|\boldsymbol{\Gamma}_{\boldsymbol{\tau}_a}(\mathbf{A}_{12}\mathbf{h}(t))\|^2 \, dt + \int_{t_2}^{t_3} \|\boldsymbol{\Gamma}_{\boldsymbol{\tau}_a}(\mathbf{A}_{23}\mathbf{h}(t))\|^2 \, dt \right.$$
$$\left. + \int_{t_3}^{t_5} \|\boldsymbol{\Gamma}_{\boldsymbol{\tau}_a}(\mathbf{A}_{35}\mathbf{h}(t))\|^2 \, dt + \int_{t_5}^{t_6} \|\boldsymbol{\Gamma}_{\boldsymbol{\tau}_a}(\mathbf{A}_{56}\mathbf{h}(t))\|^2 \, dt \right) \tag{26}$$

subject to (12)~(25)

in which the constraints, although are expressed in terms of $\mathbf{q}(t)$ $(= [\mathbf{q}_u(t)^T \ \mathbf{q}_a(t)^T]^T)$, $\mathbf{f}_g$ and $\boldsymbol{\tau}_a$ originally, can be expressed in terms of $\mathbf{q}_a(t)$ alone by (4), (5), (8), (10) and (11).

The discrete form of the optimization problem is in a standard format for nonlinear, constrained optimization in MATLAB® Optimization Toolbox, so the function *fmincon* in this package is used to solve the problem numerically. When the *fmincon* function is used to solve for the optimal $\mathbf{A}_{(\cdot)}$'s, it is found that due to the vast numbers of parameters and constraints involved, convergence of the numerical optimization is not easy to achieve. In order to obtain a convergent solution for the relevant parameters but still maintain their optimality to certain degree, three modifications are made to the optimization problem.

First of all, instead of solving for the four $\mathbf{A}_{(\cdot)}$'s matrices simultaneously, the four integrals in (26) are divided into two parts and minimized separately in a sequential manner. One of the two parts consists of the first two (stance and underactuated) phases before take-off, and the other is composed of the flight phase and the recovery phase. The sequential optimization is conducted in the way that $\mathbf{q}_{a\_23}(t_3)$ $(= \mathbf{A}_{23}\mathbf{h}(t_3))$ and $\dot{\mathbf{q}}_{a\_23}(t_3)$ $(= \mathbf{A}_{23}\dot{\mathbf{h}}(t_3))$ obtained from minimizing the first two integrals are substituted as initial conditions for the optimization of the other two integrals. With such a modification, one has to deal with only two of the four $\mathbf{A}_{(\cdot)}$'s matrices in each optimization.

Secondly, as observed from human hopping, during the underactuated phase the actuation is most intensive. Similarly

in (26), the cost associated with the underactuated phase is less penalized in order for the optimization to generate more intensive control authority during this phase. Therefore, the cost function for computing $\mathbf{A}_{12}$, $\mathbf{A}_{23}$ is modified as

$$\min_{A_{12},A_{23}} \left(\int_{t_1}^{t_2} \left\| \mathbf{\Gamma}_{\tau_a}(\mathbf{A}_{12}\mathbf{h}(t)) \right\|^2 dt + \gamma \int_{t_2}^{t_3} \left\| \mathbf{\Gamma}_{\tau_a}(\mathbf{A}_{23}\mathbf{h}(t)) \right\|^2 dt \right) \tag{27}$$

where $0 < \gamma < 1$ is a weighting factor.

The third modification is to further restrict the solution space so as to speed up the convergence of the numerical scheme. This is achieved by additionally imposing lower bound and upper bound on the CoM's take-off speed ($= \sqrt{2}\dot{z}_c(t_3)$ due to (23)) and take-off angular momentum ($H_{CoM}(t_3)$) during optimization. By the analog of projectile motion and (23), to reach a hopping distance of l, the take-off speed should be close to $\sqrt{\frac{gl}{2}}$. To avoid excessive rotation during the flight phase, the magnitude of $H_{CoM}(t_3)$ should be small. Taking these two observations into account, appropriate bounds for $\dot{z}_c(t_3)$ and $H_{CoM}(t_3)$ can be determined.

The flow chart of the final optimization procedure is depicted in Fig. 3. In this flow chart, the parameters and initial conditions needed for the optimization procedure are $\mathbf{q}_d^1$, $\mathbf{q}_d^6$, $(t_2 - t_1)$, $(t_6 - t_5)$. While the selections for $(t_2 - t_1)$ and $(t_6 - t_5)$ are quite flexible since the robot is fully actuated by motors, $\mathbf{q}_d^1$ and $\mathbf{q}_d^6$ are selected to achieve a desired hopping distance (l) and a hopping height (h) and have the same standing posture mimicking a person bending his/her body to prepare for a jump. For $\mathbf{q}_d^1$ and $\mathbf{q}_d^6$, the projection of the CoM is designed to locate around the center of the foot to assure the stability. Finally, once the flow chart produces a convergent solution, the actuated trajectories associated with the solution guarantee to achieve stability and the desired hopping distance.

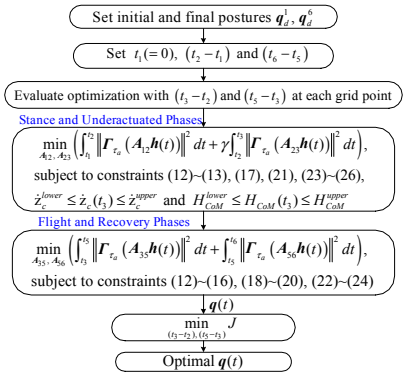

Fig. 3. The flow chart of the optimization procedure.

V. Simulations and Experimental Results

The 3-link, one-legged robot depicted in Fig. 1 is used to verify the optimization results. In the robot, the mechanical links are made of aluminum alloy, and at the ankle and the hip joints, DC servo motors (Dynamixel RX-64) are used as the actuators. Except for a gear reduction, each of the motors also integrates a potentiometer, a PID type servo-controller, and a motor driver as one module. Specifically, for verification purposes, two mechanical touch switches are respectively installed at the toe and at the heel to detect the foot-ground contact condition. A gyro sensor is attached to the foot to measure its absolute inclination angle derived by integrating the angular velocity signal. There are also Hall-effect current sensors in series with the motor coils to measure the motor currents, thus the motor torques.

A. Simulations

The optimization procedure is applied to the one-legged robot model with parameters listed in Table I, which are indentical to the geometric dimensions and the inertial properties of the robot. The position/joint angles at postures 1 and 6 are selected as $\mathbf{q}_d^1 = [0, 0, 0, 0.98, 1.28]^T$ and $\mathbf{q}_d^6 = [0.2, 0, 0, 0.98, 1.28]^T$, which implie that the robot hops on the level ground along the y direction with $l = 0.2\,\mathrm{m}$, $h = 0$. The coefficient of ground friction (μ_s) is chosen to be 3. As for the constraints in (24) and (25), $\theta_{i,\min} = \frac{20\pi}{180}\,\mathrm{rad}$, $\theta_{i,\max} = \frac{155\pi}{180}\,\mathrm{rad}$, $\frac{R}{k_m \cdot n} = 2.50\frac{\mathrm{V}}{\mathrm{N\,m}}$, $(k_e \cdot n) = 2.84\frac{\mathrm{V\,s}}{\mathrm{rad}}$ and $v = 27\,\mathrm{V}$ are obtained from the motor specifications.

TABLE I

Kinematic parameters of the one-legged robot

	foot ($i=0$)	leg ($i=1$)	torso ($i=2$)
Length l_i (m)	$l_f = 0.080$, $l_a = 0.033$	0.168	0.275
Center of mass $r_{cy,i}$ (m)	0.07	0.084	0.185
Center of mass $r_{cz,i}$ (m)	0.018	0.0	0.0
Mass m_i (kg)	0.30	0.21	0.36
Moment of inertia I_i ($\mathrm{kg\,m^2}$)	0.00012	0.00053	0.00245

Note: $l_{foot} = 0.14$ (m), width of the foot= 0.09 (m)

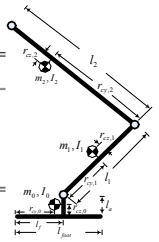

To initiate the optimization, the trajectories of actuated joints are assumed to be Bézier polynomials of order 7. The durations $(t_2 - t_1)$ and $(t_6 - t_5)$ are respectively chosen as $0.4\,\mathrm{s}$ and $0.8\,\mathrm{s}$. The weighting factor (γ) for the underactuated phase is set to 0.1. Executing the flow chart in Fig. 3 leads to the optimal $\mathbf{A}_{(\cdot)}$'s, consequently the optimal $\mathbf{q}_a(t)$. Besides, the grid search for durations of the underactuated phase and the flight phase gives $t_3 - t_2 = 0.1\,\mathrm{s}$ and $t_4 - t_3 = 0.185\,\mathrm{s}$.

The corresponding stick diagrams of the one-legged hopping robot calculated by the optimization procedure are plotted in Fig. 4(a), and the trajectory of the CoM is also plotted in Fig. 4(b). According to the figures, the robot starts statically from posture 1, in which the projection of the CoM is located around the center of the foot. During the stance phase the robot bends its torso gently to lower its CoM. Then it rapidly stretches the torso and enters the underactuated phase. With the rapid stretching in this phase, a large forward and upward reaction force from the ground is generated, so the CoM is quickly accelerated along the direction of the reaction force to initiate the takeoff. After takeoff, the CoM moves along a ballistic trajectory. In the flight phase, the robot first quickly retracts its leg to leave off

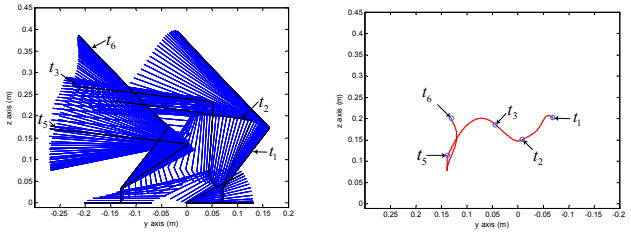

Fig. 4. (a) The consecutive stick diagrams of the optimal hop. (b) The trajectory of the CoM.

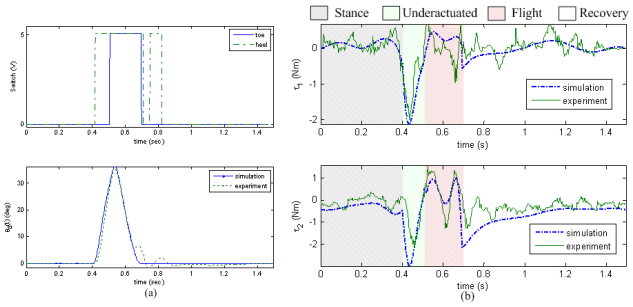

Fig. 5. (a)The histories of signals of the two touch sensors as well as the inclination angles of the foot in simulation and experiment. (b)The histories of the motors' torques in simulation and experiment.

the ground. Then the leg is extended slightly and the foot is slewed horizontally to prepare for the touch-down. After touching down, in order to support the body and prevent the robot from falling, the motions of the actuated joints produce an upward and backward reaction force from the ground so that the CoM is quickly decelerated in the vertical direction but stays around the top of the center of the foot. Finally the robot gradually recovers toward the original static posture.

B. Experiments for Stable Hop

The $\mathbf{q}_a(t)$ calculated by the optimization procedure is directly adopted as the reference trajectories for the motors' servo controllers. Experimentally, the one-legged robot can perform stable hop with a hopping distance of about $20\,\mathrm{cm}$ as the simulations. The video demonstration of the robot continuously performing three hops can be found in the website http://ldsc.pme.nthu.edu.tw/files/Hopping.

Fig. 5(a) shows the histories of signals of the two touch sensors as well as the inclination angles of the foot in simulation and experiment. In the stance phase, the foot is flatly in contact with the ground, so both touch sensors are switched off that two voltage signals are low. At about $0.4\,\mathrm{s}$, the foot starts to rotate about the toe, and the heel is lifted off the ground that the corresponding touch sensor is switched on. After a duration of about $0.09\,\mathrm{s}$, the foot is completely lifted off the ground that the robot is in flight for about $0.19\,\mathrm{s}$. Then at about $0.7\,\mathrm{s}$, the robot lands on the ground and both touch sensors are switched off again. Furthermore, the motors' torques in simulation and experiment are recorded in Fig. 5(b). Clearly, the experimental torques roughly follow the trend as the simulations.

C. Further Applications of the Optimization Procedure

Besides designing the actuation trajectories for the robot to perform stable hopping of $20\,\mathrm{cm}$ on the level ground, the proposed optimization procedure can be used to devise different hopping gaits, such as hopping with different distances or hopping up/down staircases. For example, using the computed trajectories, the robot can be demanded to hop for $10\,\mathrm{cm}$ on the level ground. Furthermore, for the robot to hop up/down staircases, the joint trajectories also can be obtained by the optimization procedure but with a modification to the constraint for clearance in (17). In order for the foot to circumvent the corner of a staircase, the constraint is modified as

$$\begin{matrix} z_0(t) \\ z_0(t) + l_{foot}\sin\theta_0(t) \end{matrix} \begin{cases} > 0, \text{ if } y_0(t) < y_s \\ > z_s, \text{ else} \end{cases} \\ , \text{for } t \in (t_3,\, t_5),$$

where (y_s, z_s) is the coordinates of the corner of the staircase. The inequalities listed respectively guarantee that both the toe and the heel do not collide with the staircase in flight. Note that the hopping height h now equals the height of the staircase z_s. Using the optimization procedure with the modified constraints, the solutions for the robot hopping up a staircase with $(y_s, z_s) = (7, 3)\,\mathrm{cm}$ and down a staircase with $(y_s, z_s) = (3, -3)\,\mathrm{cm}$ are computed. These three cases of hopping were verified by simulation and experiment. The animations of the simulations and the video demonstrations of the experiments can be also found in the website http://ldsc.pme.nthu.edu.tw/files/Hopping.

VI. Conclusions

In this paper, a one-legged robot with two actuated joints and a flat foot is developed to perform stable hop. The hopping contains a special feature that before taking off, the robot goes through an underactuated phase in which dynamic stability is violated. To exploit underactuation for effective hopping, an optimization procedure is used to systematically design the actuated joint trajectories. The feasibility of the hopping strategy and the optimal joint trajectories for stable hopping is verified by simulation and hardware implementation. Experiments indicate that the robot not only can consecutively hop on the level ground with different hopping distances but also can successfully hop up/down staircases.

References

[1] M. Raibert, H. Brown and M. Chepponis, "Experiments in Balance with a 3D One-Legged Hopping Machine," *Int. J. Robot. Res.* , 3(2): 75–92, 1984.

[2] M. Raibert, Legged Robots that Balance, Cambridge, MA: MIT Press, 1986.

[3] R. Tajima and K. Suga, "Motion having a Flight Phase: Experiments Involving a One-legged Robot," *IEEE International Conference on Intelligent Robots and Systems*, pp. 1726–1731, 2006.

[4] S. Kajita, K. Kaneko, M. Morisawa, S. Nakaoka, and H. Hirukawa, "ZMP-based Biped Running Enhanced by Toe Springs," *Proc. of the IEEE International Conference on Robotics and Automation*, pp. 3963–3969, 2007.